

Adapting to Unseen Vendor Domains for MRI Lesion Segmentation

Brandon Mac

bmac@ryerson.ca

Image Analysis in Medicine Lab (IAMLAB), Ryerson University, Toronto, ON, Canada

Alan R. Moody

alan.moody@sunnybrook.ca

Department of Medical Imaging, University of Toronto, Toronto, ON, Canada

Department of Medical Imaging, Sunnybrook Health Sciences Centre, Toronto, ON, Canada

April Khademi

akhademi@ryerson.ca

Image Analysis in Medicine Lab (IAMLAB), Ryerson University, Toronto, ON, Canada

Keenan Research Centre for Biomedical Science, St. Michael's Hospital, Toronto, ON, Canada

Institute for Biomedical Engineering, Science, and Technology (iBEST), A Partnership Between St. Michael's Hospital and Ryerson University, Toronto, Canada

Abstract

One of the key limitations in machine learning models is poor performance on data that is out of the domain of the training distribution. This is especially true for image analysis in magnetic resonance (MR) imaging, as variations in hardware and software create non-standard intensities, contrasts, and noise distributions across scanners. Recently, image translation models have been proposed to augment data across domains to create synthetic data points. In this paper, we investigate the application of an unsupervised image translation model to augment MR images from a source dataset to a target dataset. Specifically, we want to evaluate how well these models can create synthetic data points representative of the target dataset through image translation, and to see if a segmentation model trained on these synthetic data points would approach the performance of a model trained directly on the target dataset. We consider three configurations of augmentation between datasets consisting of translation between images, between scanner vendors, and from labels to images. It was found that the segmentation models trained on synthetic data from labels to images configuration yielded the closest performance to the segmentation model trained directly on the target dataset. The Dice coefficient score per each target vendor (GE, Siemens, Philips) for training on synthetic data was 0.63, 0.64, and 0.58, compared to training directly on target dataset was 0.65, 0.72, and 0.61. Our code is available at <https://github.com/IAMLAB-Ryerson/MRI-Augmentation>.

Keywords: Machine Learning, Image Translation, Data Generation, GAN, Data Augmentation, Domain Adaptation, MRI, Medical Image Analysis

1. Introduction

Imaging of white matter hyper-intensities (WMH) plays a significant role in the management, diagnosis, and evaluation of treatment of multiple sclerosis and dementia (Polman et al., 2011). Manual delineations provide important volumetric information of lesion load and spatial distributions, however they are labor intensive to acquire and are often subject to high inter- and intra-rater variability (Egger et al., 2017; Steenwijk et al., 2013). As a

result, automated lesion segmentation methods are highly sought after due to their potential to streamline clinical workflows.

In recent years, deep learning has becoming increasingly popular for medical image processing and analysis. Deep convolutional neural networks (CNNs) leverage the capacity to learn strong representations from a large amount of annotated data. However, large annotated datasets of medical images are often difficult to obtain, especially for tasks such as semantic segmentation where exhaustive pixel-wise annotations are required. Furthermore, models often perform poorly when tested on populations from outside the distribution of the training set. This is commonly referred to as domain shift problem (Gretton et al., 2008).

Domain shift is especially problematic for MR images as variations in hardware and software create non-standard intensities, contrasts, and noise distributions, which is also referred to as the multi-center (MC) effect (Reiche et al., 2019). The MC effect is known to create different image characteristics between scanners and centers even for the same patient and same tissues (Reiche et al., 2019; Zhong et al., 2012). To address domain shift, many authors have suggested utilizing domain adaptation techniques. In general, domain adaptation aims to transfer knowledge from a source domain to a target domain, typically by leveraging domain invariant features to be translated (Volpi et al., 2018; Sundaresan et al., 2021). There has been success found in various applications where a small labeled dataset was able to incorporate larger unlabeled datasets by domain adaption, which allowed for greater generalizability (Ganin et al., 2016; Wilson and Cook, 2020). While domain adaption typically seeks to learn invariant features from real data, there have been recent developments in the application of generative adversarial networks (GAN) to create synthetic data. The objective of GANs is to generate synthetic data representative of a target distribution. This is achieved through adversarial training of a pair of generator and discriminator models, in which the generator captures the data distribution, and the discriminator estimates the probability that the data is real or generated (Goodfellow et al., 2014). The capacity to generate synthetic data points have lead authors to explore the prospect of utilizing these methods to augment limited data sets (Sandfort et al., 2019; Frid-Adar et al., 2018; Huo et al., 2019).

A promising trend of medical applications building upon CycleGAN (Zhu et al., 2020) have emerged for cross-modal synthesis from unpaired training images. In Zhang et al. (2019) and Huo et al. (2019), the authors have demonstrated the capacity to utilize cycle-based methods to augment between MR and CT images for both data synthesis and segmentation. By having a pair of generator and discriminator networks learn the respective distributions of each domain, synthetic data points can be generated through image translation from one domain to another. The experimental results from these works have shown the capacity for the translation to be annotation-preserving in the application of semantic segmentation. Building upon this, rather than the application of cross-domain translation between modalities, in this paper we investigate the application of image translation models to MR images between scanner domains to address the MC problem.

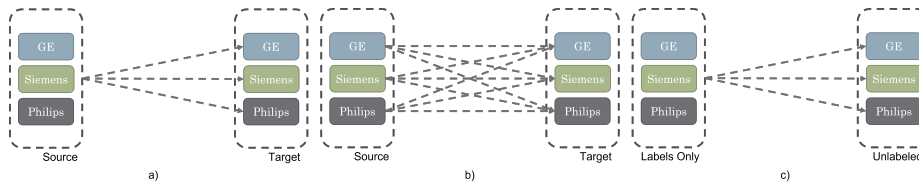


Figure 1: Image-translation modes to be investigated. a) Image2Image translation, b) Scan2Scan, c) Label2Image

1.1 Contribution

In this work, image translation techniques are utilized to augment MR images from one scanner domain to another for the purposes of semantic segmentation. Specifically, we seek to evaluate the capacity of these techniques to translate images from a source domain to create synthetic data points representative of the target domain. Rather than generalization, the objective is to see how well these images represent the target domain, and if training a segmentation model to learn from these synthetic images is comparable to a segmentation model learning directly from the target domain. We take inspiration from the work of Zhang et al. (2019) and Huo et al. (2019) for cross-modal synthesis between MR and CT modalities, however apply these techniques to cross-domain translation between MR scanners. To elaborate, our investigation consists of two multi-center MR image datasets, from which we designate one as our source dataset and the other as our target dataset. We further separate the target dataset by the respective vendors (GE, Siemens, and Philips) and consider each as individual target distribution. For our experiments, we consider the following cases to be explored for defining the source distribution:

- Image2Image - Translation from multi-center distribution to target distribution
- Scan2Scan - Vendor specific translation from source to target distribution
- Label2Image - Unpaired label to image translation from source to target distribution

Figure 1 provides an illustration of the image translation cases. The overall objective was to define the optimal configuration to generate synthetic samples in a target domain through image translation. Image2Image utilizes the entire source dataset to train a translation model to each of the respective target distributions. This was to observe if the multi-center effect would translate to a specific target distribution. Contrasting this, Scan2Scan separates the source dataset by the respective vendors and trains a translation model per specific combination of source-target vendor pairs (i.e. GE2GE, Siemens2Philips, and Philips2GE). Lastly in Label2Image, we investigate defining the source distribution as the label images from the source dataset, and explore the potential of training a translation model for unpaired segmentation annotations to images in each target domain. From these models, we then consider two sets of experiments for training the segmentation models on synthetic data to further explore the multi-center effect. We define the synthetic datasets per method as the following:

- Generate synthetic data representative of a single target distribution
- Pool the synthetic data from each target distribution together to create a synthetic multi-center dataset

Our investigations found that the multi-center effect had little change on the quality of the synthetic images for image-to-image translation (Image2Image and Scan2Scan), however, did impact the overall variance of the segmentation performance. It was found that Label2Image mode yielded the best results for generating synthetic data for segmentation training, with results comparable to training directly on the target distribution. Interestingly, while the Label2Image synthetic data did train segmentation models better, it was noted that Label2Image yielded images that were relatively less realistic than the other modes. To explore the relationship between realism and effective training data further, we also conduct an experiment generating synthetic source labels using DCGAN (Radford et al., 2016) to translate to the respective target distributions.

2. Related Works

This work involves various aspects of medical image analysis, domain adaption, and generative adaptive networks (GANs). In the following sections, an overview of the relevant works is presented.

2.1 Semantic Segmentation

Recent advances in semantic segmentation have largely been dominated by deep learning methodologies (Khademi et al., 2021). Notably, the most common methods are based on fully convolutional networks (FCNs). Long et al. (2015) demonstrated one can effectively transform any CNN model to an FCN. In medical applications, the most common FCN is encoder-decoder style U-Net first proposed by Ronneberger et al. (2015). Exemplifying this, the top 11 teams participating in the MICCAI 2017 Grand Challenge for automated WMH segmentation used some form of U-Net architecture (Kuijf et al., 2019). However, it is usually expensive and difficult to acquire pixel-level annotations. Coupled with this, it is known that these models perform well on populations sampled from the training distribution, but perform poorly on out-of-domain populations (Volpi et al., 2018). To address this, authors have proposed solutions such as weak supervision, where weak labels such as bounding boxes (Khoreva et al., 2016), object localization (Qi et al., 2016), and point supervision Bearman et al. (2016), to then refine to pixel-wise predictions. However, weak supervision does not perform as well as supervised methods as it is difficult to approximate boundary information from weak labels (Hung et al., 2018).

2.2 Domain Adaptation

To address the issues above, various domain adaption methods have been proposed to incorporate unlabeled data with labeled datasets. In general, domain adaption methods attempt to transfer knowledge from a source domain to a target domain by leveraging domain invariant features (Wilson and Cook, 2020). A common technique is transfer learning, in which low level features are frozen, while higher level features are fine tuned (Ghafoorian et al.,

2017). However, the performance is often known to rely on sufficient initial training data to be robust. Another domain adaption model is DANN, which consists of a feature extractor, a domain predictor and a label predictor (Ganin et al., 2016). The adversarial nature of the network is the gradient reversing layer between the domain predictor and the feature extractor, in which the labels prediction is minimized, while the domain predictor maximized. Similarly, an alternative is presented in domain unlearning, in which the method involves learning the domain prediction for a fixed feature representation, and then minimizing the domain shift, while maximizing in domain confusion (Dinsdale et al., 2021).

2.3 Generative Adversarial Networks

Recent developments in generative adversarial networks (GANs) (Goodfellow et al., 2014) have shown a variety of applications. As mentioned earlier, adversarial networks have been applied to domain adaptation (Ganin et al., 2016). Hung et al. (2018) demonstrate the application of adversarial networks for semi-supervised training of semantic segmentation models. For data generation, application in the medical domain has been demonstrated by Frid-Adar et al. (2018) to generate synthetic liver images to improve lesion classification. In Li et al. (2021), the authors propose a network to model the joint image-label distribution, and synthesis of both image and semantic mask. Similarly, Zhang et al. (2021) proposes training on a small labeled set and disentangling the latent space of StyleGAN (Karras et al., 2019) architecture to generate synthetic labeled datasets. However, the authors note that the requirement is highly detailed semantic labels.

Several authors have proposed utilizing CycleGAN (Zhu et al., 2020) as a method to adapt images from one domain to another for the purpose of augmenting training data. Translation from MR to CT domains have been demonstrated by several authors (Wolterink et al., 2017; Zhang et al., 2019; Jiang et al., 2018). The original authors of CycleGAN have demonstrated the capacity to synthesize realistic images from label information (Zhu et al., 2020), in a similar fashion to conditional GANs (Isola et al., 2018). A similar work to our investigation, Palladino et al. (2020) utilize CycleGANs to translate between scanner vendors within the MICCAI 2017 WML Grand Challenge data (Kuijf et al., 2019). However, in their implementation, they train only on real data and use the image translation models to augment the images the training distribution during testing.

3. Methods

An overview of the training setup is shown in Figure 2. Details regarding pre-processing, data, architecture and evaluation metric can be found below.

3.1 Pre-Processing

Brain volumes were first skull stripped using method proposed by DiGregorio et al. (2021) to estimate the intracranial volume. Masks generated by the mentioned method were then used as a label along with WML labels for the source dataset. After stripping the skull, the whole volume was normalized to an intensity between 0 and 1 by dividing by maximum intensity. From the volume, axial slices were taken and resampled to 256 x 256 using default resize parameters in python scikit-image library (Van der Walt et al., 2014). Slices that

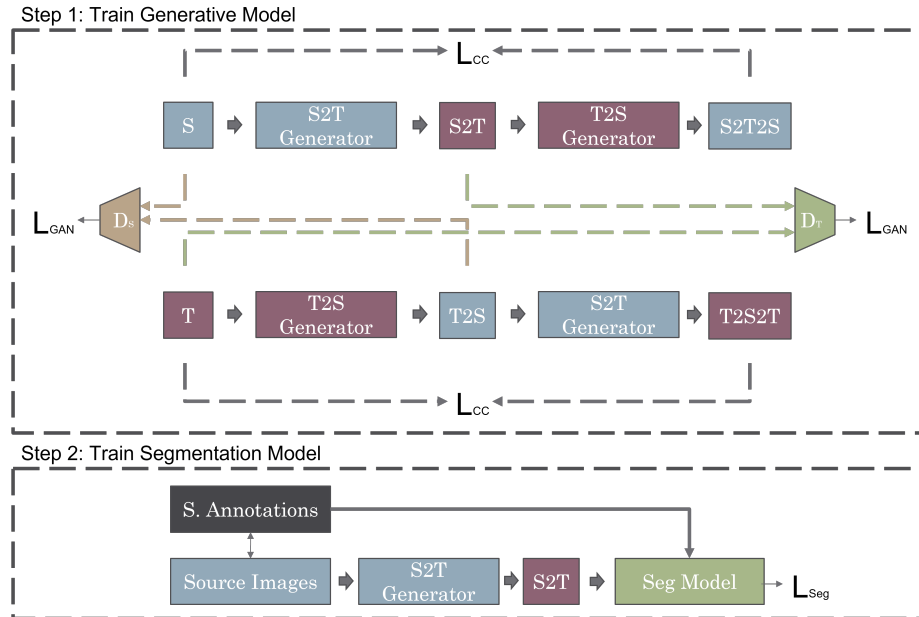


Figure 2: Outline of Training Setup

contained brain images with pixels that have less than 10% of the volume or were empty were discarded. This resulted in the upper- and lower-most slices being discarded, which were considered acceptable as those regions were not expected to contain lesions (and had hardly any brain tissue) (Wardlaw et al., 2015). This was done to ensure that when training the translation models that they do not mode collapse to empty slices. Some moderate augmentations were applied to the images during training, including random scaling, rotation, and mirroring.

3.2 Data

Two multi-center MR image datasets were used in our experiments, from which we designate one as our source dataset and the other as our target dataset. The source data consists of 60 FLAIR volumes publicly released by the MICCAI 2017 Grand Challenge for WMH segmentation (Kuijff et al., 2019). We designate the MICCAI dataset as the source dataset, as the annotations are considered the gold standard due to the multiple expert raters per annotations. The target dataset consists of 54 FLAIR volumes from the Canadian Atherosclerosis Imaging Network (CAIN) and is a pan-Canadian effort to study vascular disease (Tardif et al., 2013), with WML labels generated by experienced raters (Khademi et al., 2021). The labels belonging to CAIN were not used in any training, and were strictly reserved for validation.

A summary of the total number of images after pre-processing for both source and target distributions can be found in Table 1. In the table, the data is split into the respective scanner vendors. For training the image translation models, we pool the data as per each mode defined above in Figure 1. Regarding Image2Image and Label2Image, all images and labels (respective of each mode) from the source (MICCAI) distribution were pooled

together as a set containing 1,695 images. From this set, individual translation models were trained to translate to each of the vendors in the target distribution (341 images in GE, 574 in Siemens, 767 images in Philips). For Scan2Scan, a image translation model was trained on each combination of source vendor to target vendor. For example, some of the image translation models trained were GE-to-GE (538 to 341 images), GE-Siemens (538 to 574 images), and GE-to-Philips (538 to 767 images). A summary of all the combinations can be found in Appendix under Table 3

Source: MICCAI				
Centers	Scanner Vendors	Total	No. Labels	No. Images
Amsterdam	GE	20	20	538
Singapore	Siemens	20	20	554
Utrecht	Philips	20	20	603
Target: CAIN				
176, 202	GE	10	10	341
190, 1180, 1203	Siemens	18	10	574
198, 320	Philips	26	10	767

Table 1: Dataset Summary

3.3 Architecture

In Figure 2, S denotes the source dataset with annotations and T denotes the target dataset without annotations. The generators used consists of three convolution blocks with a stride of 2 and three ResNet blocks, as defined by Zhu et al. (2020) and He et al. (2015). Modifications to number of ResNet blocks were to reduce the parameter space to better suit the smaller number of images. The segmentation model is a modification of the U-Net (Ronneberger et al., 2015), consisting of five ResNet blocks (He et al., 2015) in the encoder path, and mirrored with 2D transposed layers in the decoding path, with a single ResNet block as the bottleneck.

3.3.1 LOSS FUNCTIONS

For training CycleGANs, the loss function consists of two main components. First is the adversarial loss defined as the following:

$$\mathcal{L}_{GAN}(G, D, A, B) = \mathbb{E}_{y \sim B} [\log D(y)] + \mathbb{E}_{x \sim A} [1 - \log D(G(x))] \quad (1)$$

Where, the generator attempts to generate images that approximates the real images, and the discriminator attempts to differentiate between generated and real. Second is the cycle consistency loss defined as the following:

$$\mathcal{L}_{cycle}(G_{A2B}, G_{B2A}, A) = \mathbb{E}_{x \sim A} |G_{B2A}(G_{A2B}(x)) - x|_1 \quad (2)$$

The cycle consistency loss is a reconstruction loss following the translation through paired generators. The total loss function is defined as the following for a paired generator and discriminator:

$$\mathcal{L}_{Total}(G_{S2T}, G_{T2S}, S, T) = \lambda_1 \mathcal{L}_{GAN}(G_{S2T}, G_{T2S}, S, T) + \lambda_2 \mathcal{L}_{GAN}(G_{T2S}, G_{S2T}, T, S) \quad (3) \\ + \lambda_3 \mathcal{L}_{Cycle}(G_{S2T}, G_{T2S}, S) + \lambda_4 \mathcal{L}_{Cycle}(G_{T2S}, G_{S2T}, T)$$

For all modes, we utilize the default parameters as defined in original CycleGAN (Zhu et al., 2020) for the lambda weighting in equation 3. For the segmentation models, we utilize generalized Dice loss (Sudre et al., 2017) due to the relative class imbalance of white matter lesions in the images.

$$\mathcal{L}_{seg} = 1 - 2 \frac{\sum_{l=1}^2 w_l \sum_n r_{ln} p_{ln}}{\sum_{l=1}^2 w_l \sum_n r_{ln} + p_{ln}} \quad (4)$$

Where, r represents the real annotations and p represents the predictions. The weighting coefficient, $w_l = \frac{1}{(\sum_{n=1}^N r_{ln})^2}$, is used to correct the contribution of each class by the inverse of the volume.

3.3.2 TRAINING

For each of the image translation modes, we define the source and target distributions of the data by the different modes (Image2Image, Scan2Scan, and Label2Image). A summary of the different configurations can be found in Appendix under Table 3. For each experiment, we train for 50 epochs with the last 25 epochs applying learning rate decay to 0 (You et al., 2019), with an initial learning rate of 0.0002. For increasing stability, we train our discriminators with memory of eight images (Shrivastava et al., 2017). The size of the batches was 4. As mentioned above, we attempt to further explore the application of Label2Image translation by attempting to utilize synthetically generated labels. To accomplish this, we train a DCGAN (Radford et al., 2016) model using the default parameters to model the label images. Once trained, we sample 5000 images from the generator and use it as a source domain, and repeat the above experiment.

Once the image translation models are trained, we conduct two sets of experiments for training segmentation model. The first set is creating a synthetic dataset per mode for each target distribution. For example, for Scan2Scan models that were trained with GE volumes as the target dataset, the synthetic data generated was pooled together to create a synthetic dataset. The second set consists creating multi-center synthetic dataset per mode by pooling the generated data together. For example, for the Label2Image models, the synthetic data from all the different target distributions were pooled together to make a synthetic multi-center dataset.

The segmentation models were trained in a supervised fashion on the synthetic data with the annotations from the source domain, as shown in Figure 2. Only the lesions annotations were used in training. For each model, we train on 50 epochs with a batch size of 8, and utilizing Adam optimizer (Kingma and Ba, 2017) ($\beta_1 = 0.5$, and $\beta_2 = 0.999$) with an initial learning rate of 0.001.

We repeat the segmentation training configuration to establish our baseline performance, in which we seek define a lower and upper bound. The lower bound is defined as performance

of the segmentation model trained on only the source domain and tested on the target domain. This is to approximate the effect of the domain shift across different distributions. The upper bound seeks to define the performance of a segmentation model trained and tested on the target distribution data. In other words, the upper bound seeks to observe a model that is potentially over-fitted to the training data.

3.4 Evaluation Metrics

To evaluate segmentation performance we utilize six evaluation metrics to compare the WML prediction masks to the ground truths. Five of the metrics are derived from standardized metrics purposed by the MICCAI 2017 WMH Segmentation Grand Challenge; Dice Similarity Coefficient (DSC), Hausdorff distance (HD), Average Volume Difference (AVD), Lesion Recall (L-Recall), and Lesion F1 (L-F1) (Kuijf et al., 2019). We also include False Positive Rate (FPR) as a percentage, since there is a significant imbalance of positive classes (lesion) and negative classes (foreground).

One of the standard metrics to measure the quality of generated images is to utilize Fréchet inception distance (FID), which compares the Wasserstein-2 distance between two Gaussians of the feature representation defined by InceptionV3 pretrained on ImageNet (Heusel et al., 2018). It has been found lower scores were tended to correlate to human agreement (Lucic et al., 2018). The formulation of FID score is given by the following:

$$FID = |m - m_w|^2 + Tr(C + C_w - 2(CC_w)^{\frac{1}{2}}) \quad (5)$$

Where, the features are sampled from the coding layers in the InceptionV3 network, and the respective mean and co-variance are calculated for the generated images, (m, C) and real world images (m_w, C_w) . FID score is typically calculated on sufficiently large data sets, as the estimation of the co-variance matrix requires sufficient number of samples relative to the vector length of the feature vector (2048 for original implementation). As we do not have sufficient number of samples, in this paper we explore sampling the feature vector at different depths of the network. Inspired by FID score implementation by Seitzer (2020) we sample at; first max pooling features (64), second max pooling features (192), pre-auxiliary classifier (768), and final averaging pooling features (2048). While FID score is calculated using a model pre-trained on natural images may raise concerns of applicability to MR images, the objective of utilizing the metric is to have an objective feature representation to compare between the different models.

4. Results

In the following, the results of experiments are presented. We examine visually the quality of the augmented data, the segmentation performance of the model trained on the augmented data, and lastly a quantitative comparison using FID score.

4.1 Augmented Data

Figure 3 shows a sample of augmentation across scanner domains. On the left, the original images are sampled from each of the centers in the source domain (MICCAI), displaying the respective MR image and mask. For the segmentation mask, white indicates WML and

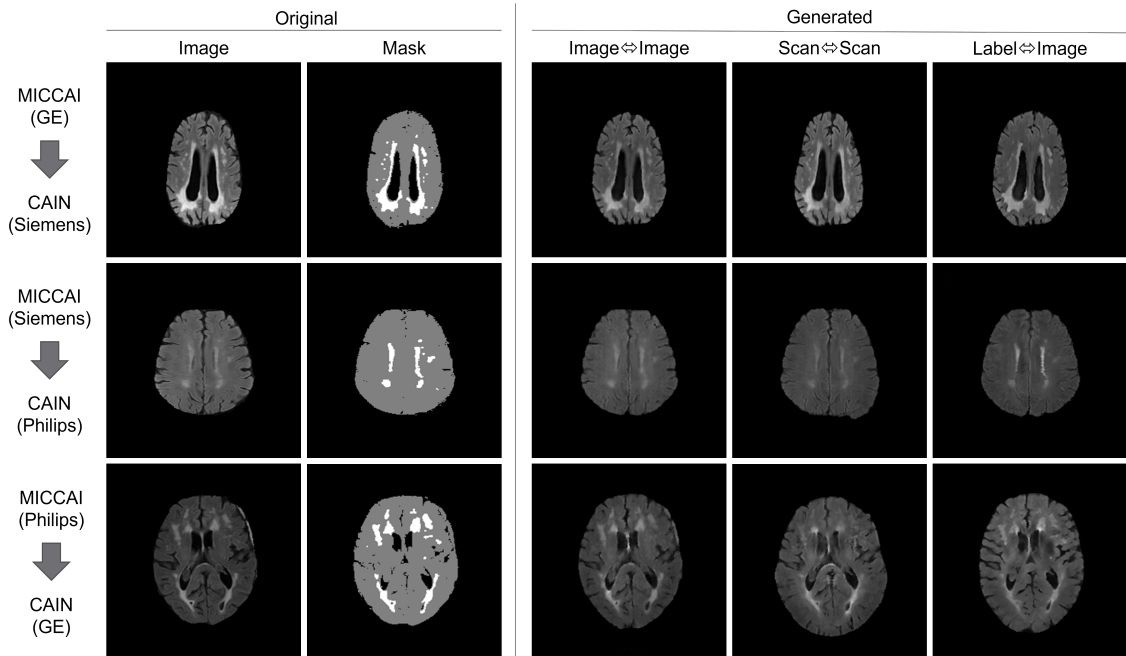


Figure 3: Example of Augmentation from Multiple Priors

gray indicates brain. The augmented images on the right are the results of each translation, after augmentation they are reshaped back into the original dimension of the source image.

Warping is present for both Image2Image and Scan2Scan modes. For example, in Figure 3, for translation between GE and Siemens, the resultant images for the two modes yields warping of the brain region when compared to original image. This is likely an artifact from augmenting from an image that has a significantly different aspect ratio. The example shown in Figure 4, shows less of this particular warping due to the source image being closer to 1:1 aspect ratio. For Scan2Scan, there appears to be cases in where the labels are not maintained through translation, as shown in Philips to Siemens translation (center image) in Figure 4. The Label2Image translation appears to be the most consistent in terms of overall shape and label consistency. Figure 3 and 4 both show relatively realistic appearing images. However, some anatomically incorrect gyri appear in the example in the Philips to GE translation (top right) in Figure 4.

4.1.1 AUGMENTATION FROM SYNTHETIC LABELS

Extending the investigation of utilizing labels as priors for translation, Figure 5 displays the results of the synthetic labels generated on the left and the resultant translation to each domain on the right. As with examples shown in Figure 3 and 4, the overall shape and label consistency is maintained relative to original input, performing similarly to Label2Image in the above section. Overall brain images appear to be easily discernible as generated images. Some portions of the generation appears less textured than what is typically expected in real images as well, leading to suggestion that the model may be overgeneralizing.

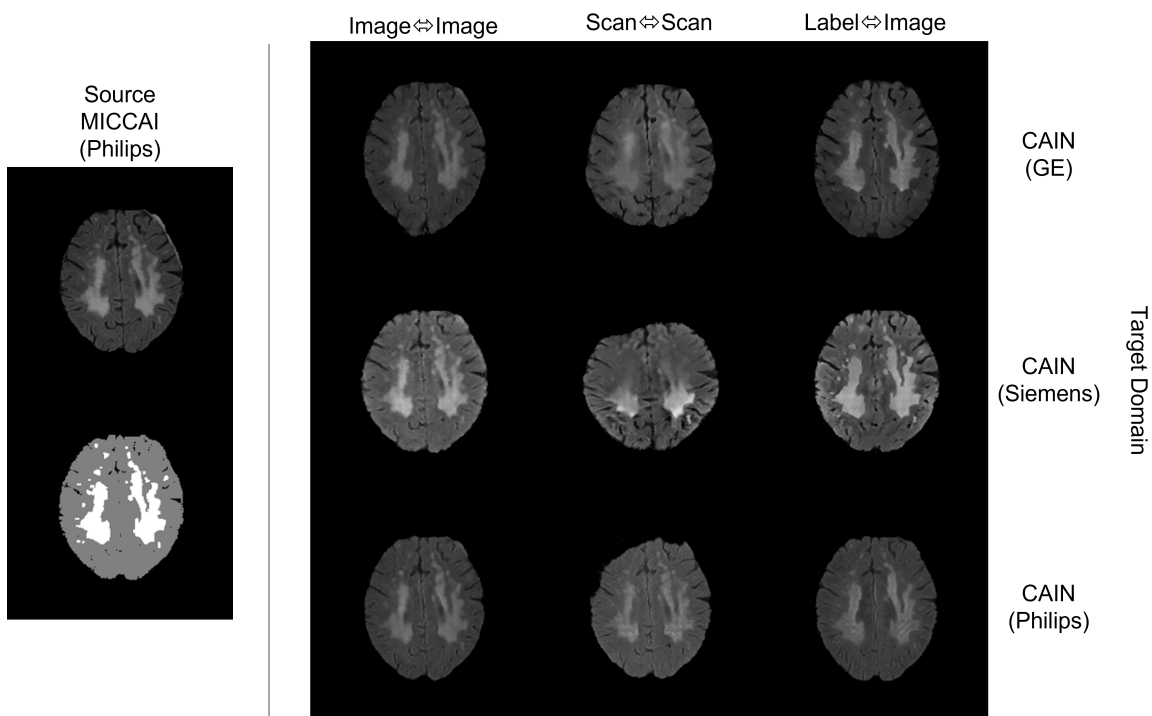


Figure 4: Example of Augmentation from Single Prior

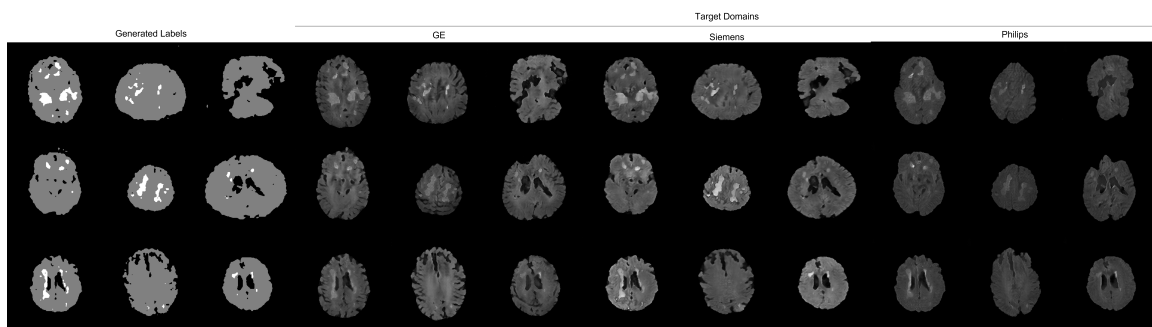


Figure 5: Synthetic Labels to Target Domains

4.2 Segmentation Performance

4.2.1 TRAINING ON TARGET DISTRIBUTION

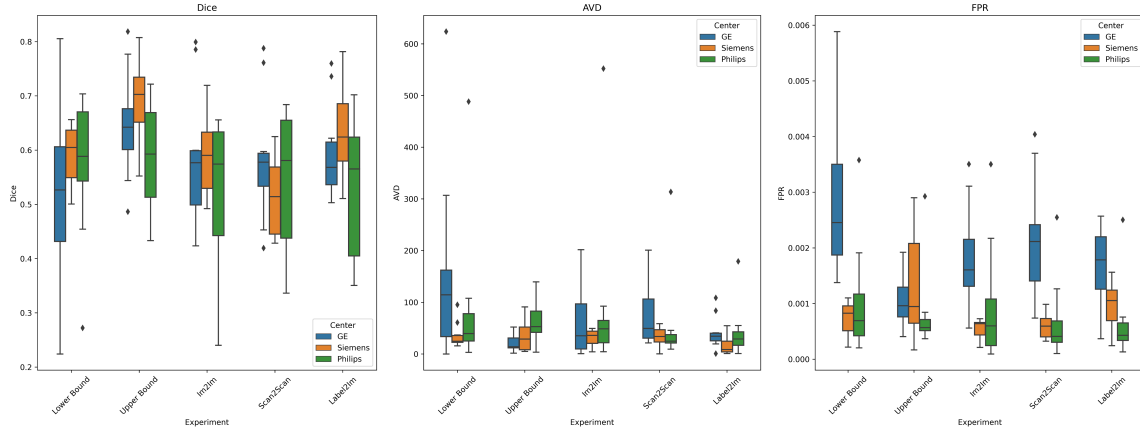


Figure 6: Segmentation Performance for Single Domain

In this section, the results for the set of experiments where segmentation models were trained on synthetic data derived from a single scanner in the target distribution will be analyzed in the context of lesion segmentation. For each augmentation mode, the segmentation performance for each scanner vendor is shown in Figure 6. Observing the overall trend in Figure 6, across all the models, there appears to be significant improvement when comparing performance of segmentation on GE volumes to the lower bound. There appears to be slight improvement in segmentation on Siemens volumes for Image2Image and Label2Image models, with notable performance of Label2Image performance being similar to upper bound performance. Dice similarity performance for Philips volumes appears to have worsened across all models, however AVD and FPR still show positive results with low scores for Philips. In Table 5 the performance of the individual models are summarized for the respective metrics. Also within Table 5, we show segmentation results where we have taken the liberty to explore the possibility of utilizing CycleGANs as a form of unsupervised segmentation model for the Label2Image models. Since, for the training of Label2Image, there exists a Label2Image model that is paired with it, which acts in a similar fashion as training segmentation. However, the segmentation provided in this unsupervised manner was not viable, as the average Dice coefficients scores were 0.44, 0.37, and 0.32 for the respective scanners (GE, Siemens, Philips).

4.2.2 TRAINING ON MIXED DISTRIBUTION

In the following, the lesion segmentation performance will be analysed for the set of experiments where segmentation models were trained on synthetic multi-center data, for which synthetic data generated by each augmentation mode were pooled together. For each augmentation mode, the segmentation performance for each scanner vendor is shown in Figure 7. It was expected that there would be improvement to the upper bound performance due to larger dataset. Comparing Figure 6 and 7, for the Image2Image and Scan2Scan models,

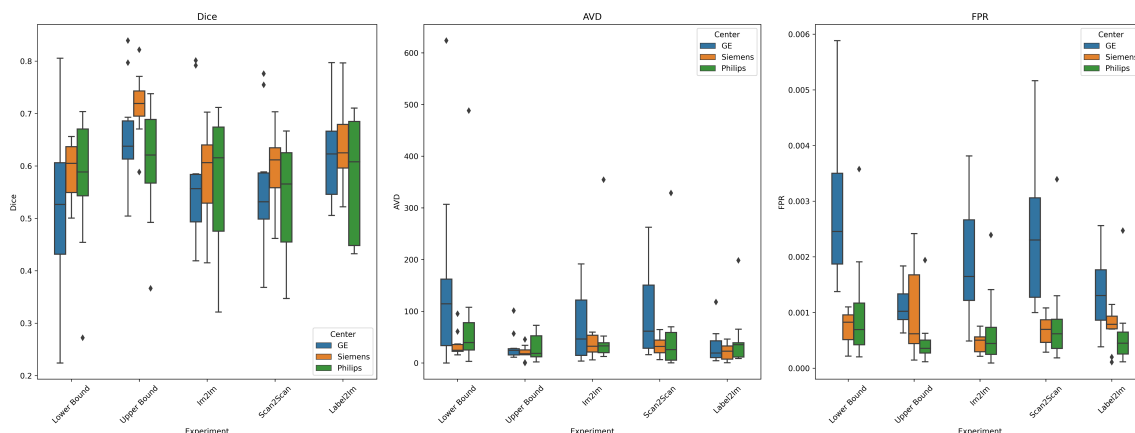


Figure 7: Segmentation Performance for Mixed Domain

there appears to be no significant improvement on GE and Siemens domains, however performance on Philips did improve slightly. Notably, the performance of the models trained on label-to-image models show significant improvement on GE and Philips domains, with 0.04 and 0.05 improvement respectively on DSC, with a minor improvement on Siemens domain, with an improvement of 0.01. In Figure 8, we present the relative consistency between scanner vendors for each mode as a function of coefficient of variation (COV), which is defined as the ratio of the standard deviation to the mean (Everitt and Skronidal, 2002). We observe that for each mode we investigated, there is significant decrease in overall COV relative to the COV of the lower bound, indicating an overall improvement to consistency.

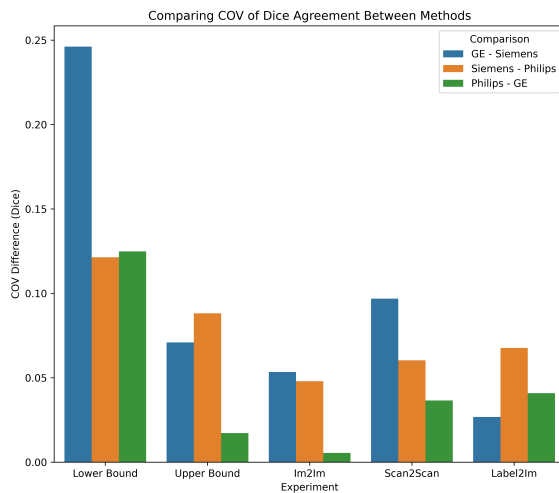


Figure 8: Comparison of COV between centers for each method

The results above imply that the Label2Image is the optimal mode for image translation in context of generating synthetic samples for segmentation training. Exploring this implication further, the experiments were repeated for the data generated in Figure 5. The

results presented in Appendix under Table 6 show that these series of experiments did not yield good segmentation performance, with average Dice coefficients of 0.40, 0.40, and 0.32 for GE, Siemens, and Philips respectively compared to Dice coefficient averages by Label2Image of 0.63, 0.64, and 0.58.

4.3 FID and Visualization

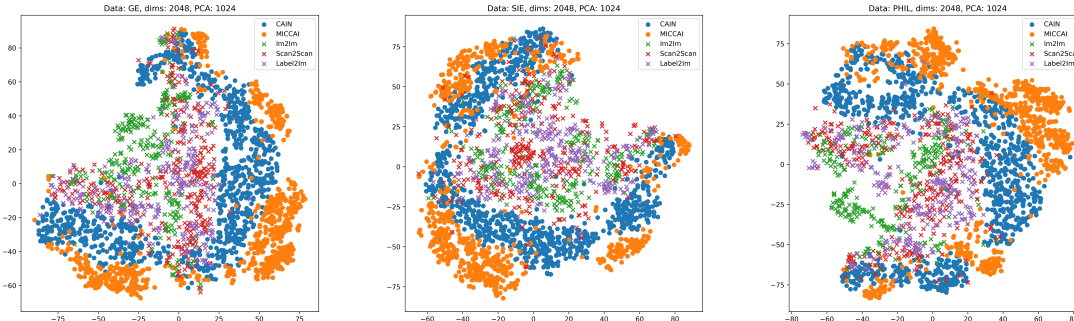


Figure 9: T-SNE Visualization

Analysis in the following attempts to quantify the visual quality between the augmentation modes as compared to the real images from the target (CAIN) distribution. Table 2 shows the FID scores relative to the target (CAIN) distribution of each of the modes and the source (MICCAI) dataset at different depths of the InceptionV3 network. The exploration of different depths was to observe the comparison of the features at different levels of complexity (with lower layers consisting of low complexity features, to more complex features at later layers). We observe the scores of Image2Image mode appears to have the highest FID score for the deeper layers, even when comparing to scores generated by MICCAI. Scan2Scan images appear to have the lowest FID scores, possibly indicating the images being closer to the target distribution.

Figure 9, shows a visualization of the features sampled at the final averaging pooling features using T-SNE (Van der Maaten and Hinton, 2008). Since the images are MR images, the expected natural image features are likely to be redundant and not applicable, thus we first utilize PCA to reduce the dimensions from 2048 to 1024 (Jolliffe and Cadima, 2016). For each of the domains, the generated images tend to be cluster around each other, while being closer to the target (CAIN) distribution, while being further from source dataset (MICCAI).

5. Discussion

It was demonstrated that data points representative of a target dataset can be generated through augmenting a source dataset through image translation. By augmenting the data and reusing the annotation labels, we found that it is possible to approach segmentation performance defined by the upper bound model (trained on the target distribution directly). Our investigation found that synthetic data generated from label images yielded results

Method	FID: 64	FID: 128	FID: 768	FID: 2048
Image2Image	0.017	0.299	0.161	65.129
Scan2scan	0.012	0.164	0.091	36.493
Label2Image	0.014	0.154	0.097	39.393
MICCAI	0.318	1.289	0.146	46.975

Table 2: Modified FID score along different vector lengths

comparable to segmentation models trained directly on the target dataset. In this section, we discuss further on the multi-center effect, comparison between label versus real images as priors, and the importance of realism in training.

5.1 The Multi-Center Effect

It was expected that multi-center data would have increased variability due to the multi-center effect. We observe this in Figures 6 and 7, when observing the upper bound model (which was trained directly on the target dataset) having higher variability in segmentation performance in terms of Dice coefficient agreement. The higher variability can be understood as the problem of concept drift (Zenisek et al., 2019), in where systems become less accurate over time as more data is introduced. However, this effect is not well understood in context of image synthesis. We attempt to observe this effect by changing the variability of the source datasets for the case of Image2Image and Scan2Scan. Presented in Figure 3 and 4, the generated samples of Image2Image and Scan2Scan can be observed to create relatively realistic images that are difficult to discern visually which are better. Observing the segmentation performance of models trained on this data in Figure 6 and 7 show similar Dice agreement between Image2Image and Scan2Scan models. Therefore, it may be inconclusive whether the multi-center effect is present in image synthesis for the case presented in this paper. However, the relative amount of data used in training may suggest overfitting in generative models. In study by Karras et al. (2020), generative models were monitored by their FID score to a test set and varied by the amount of data used in training. It was found that models with less training data tended to overfit, as the FID scores diverged at earlier points than models trained with more data. From this we can infer that the generated images tended to contain features more specific to the training set, and in which we observe this in Table 2, where Scan2Scan models show significantly lower FID scores than Image2Image models.

5.2 Label versus Images as Priors

The cycle consistency introduced in CycleGAN (Zhu et al., 2020) regularizes the training of the model by enforcing the translation $G_{B2A}(G_{A2B}(x)) \approx x$. What this infers, is that information and features in image x is encoded by $G_{A2B}(\cdot)$, such that it can be decoded by the paired network, $G_{B2A}(\cdot)$. For both Image2Image and Scan2Scan modes, as their image priors were real images, the expected information maintained through translation would cause the generated images to be similar. We can observe the relative similarity to the prior images for Image2Image and Scan2Scan modes in Figure 3 and 4. However,

despite the generated samples being more similar to real images, Figure 6 and 7 show that segmentation models trained on Label2Image performed better in every segmentation metric and approximates better to the performance of model trained directly on target data. One suggestion of why Label2Image data perform better is that the label image priors are less complex and contain less information than real priors. Lower complexity means that less features have to be maintained in the translation of $G_{A2B}(x) = x'$, and features in synthetic image x' primarily consist of features learned of the target distribution. Another reason may be due to the function of the decoder network to maintain label consistency. Since the forward path, $G_{A2B}(x) = x'$, creates a synthetic MR image, the decoder path, $G_{A2B}(x') = x$, translates the synthetic image back to label domain. In effect, the decoder path functions similarly to a segmentation model. Since the decoder path functions similarly as a segmentation model, this opens up the consideration of unsupervised learning for segmentation. However, we evaluate the decoders respective of each model for Label2Image in Appendix under Table 5 as a function of segmentation performance and was found that unsatisfactory results, with unsupervised performance scoring lower than our segmentation model trained on out-of-domain data.

5.3 Realism in Training

Relative to images generated by Image2Image and Scan2Scan modes, Label2Image data appears to be less realistic, with overgeneralized textures and implausible structures appearing in generated data. This is likely due to the label image priors containing less details and are therefore less restrictive in translation. Despite this, the segmentation models trained on Label2Image data had the highest performance. It may be suggested that by training on overgeneralized images, the segmentation model is better trained to learn features of the target distribution. To explain further, this could be due to the operations of convolution layers in neural networks, as the overall receptive field is activated when a learned feature is "detected", the relative location within the receptive field may not matter. To observe the limits of this, we experimented with generating synthetic labels and using them as priors for Label2Image translation. Figure 5 shows a sample of the synthetic labels translated to each respective target distribution. In these samples, the generated images are less realistic and contain more implausible structures. The results of the training of these generated data can be found in Appendix under Table 6. The segmentation performance of models trained with this data was lower than the model trained on out-of-domain data, suggesting there may be a minimum requirement to realism that needs to be met.

6. Conclusion

In this paper, it was demonstrated that CycleGAN (Zhu et al., 2020) can be implemented to create synthetic data points representative of a target dataset through image translation, and said data points can be used to train segmentation models. Specifically, we considered the application for augmentation between MR dataset, and investigate the particular configurations of the distributions between source and target. The performance of these segmentation models have shown to approach performances similar to segmentation models trained directly on the target dataset. It was observed that the optimal configuration is to utilize label images as a prior to create synthetic data points, despite the generated images

being less realistic and overgeneralized. Future work intends to explore the relationship between realism in synthetic data and applicability in augmenting small datasets. Potential applications could be found in topics such as active learning, adversarial attacks, and pseudo-labeling. Within the clinical setting, training data representative of a particular vendor or center could potentially be readily generated from a few samples. In turn, this could reduce the overhead required to train robust algorithms and make the overall process of integration more scalable.

Acknowledgments

We thank NSERC Discovery Grant Program for funding this research.

Ethical Standards

The work follows appropriate ethical standards in conducting research and writing the manuscript, following all applicable laws and regulations regarding treatment of animals or human subjects.

Conflicts of Interest

We declare we don't have conflicts of interest.

Appendix A.

.1 Segmentation Model

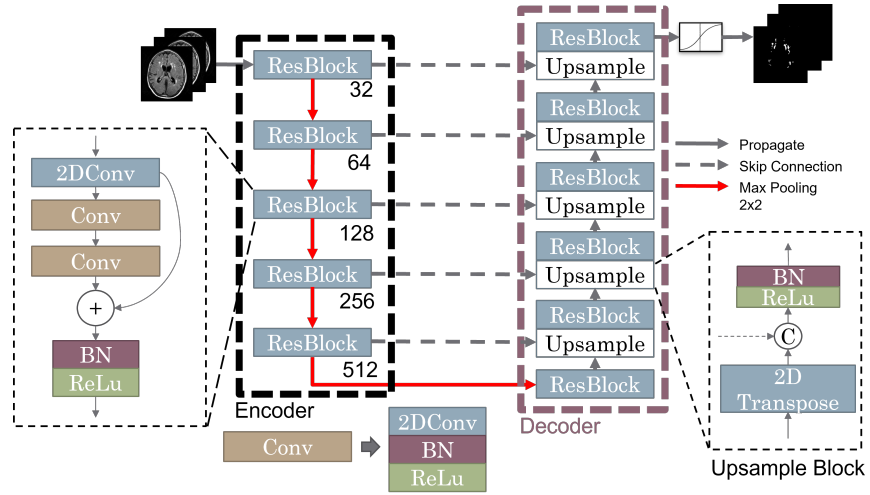


Figure 10: Segmentation Model

.2 Data Table for Each Experiment

Mode	Source	No. Images	Target	No. Images
Image2Image	MICCAI	1695	CAIN: GE	341
Image2Image	MICCAI	1695	CAIN: Simens	574
Image2Image	MICCAI	1695	CAIN: Philips	767
Scan2Scan	MICCAI: GE	538	CAIN: GE	341
Scan2Scan	MICCAI: GE	538	CAIN: Siemens	574
Scan2Scan	MICCAI: GE	538	CAIN: Philips	767
Scan2Scan	MICCAI: Siemens	554	CAIN: GE	341
Scan2Scan	MICCAI: Siemens	554	CAIN: Simens	574
Scan2Scan	MICCAI: Siemens	554	CAIN: Philips	767
Scan2Scan	MICCAI: Philips	603	CAIN: GE	341
Scan2Scan	MICCAI: Philips	603	CAIN: Simens	574
Scan2Scan	MICCAI: Philips	603	CAIN: Philips	767
Label2Image	MICCAI: Labels	1695	CAIN: GE	341
Label2Image	MICCAI: Labels	1695	CAIN: Simens	574
Label2Image	MICCAI: Labels	1695	CAIN: Philips	767
DCGAN	N/A	N/A	MICCAI: Labels	1695
Syn2Image	Syn Labels	5000	CAIN: GE	341
Syn2Image	Syn Labels	5000	CAIN: Simens	574
Syn2Image	Syn Labels	5000	CAIN: Philips	767

Table 3: Summary of Data Splits for GAN Training

Single Target Distribution		
Mode	Sources	No. Images
Image2Image	MICCAI → CAIN: GE (1695)	1695
Image2Image	MICCAI → CAIN: Siemens (1695)	1695
Image2Image	MICCAI → CAIN: Philips (1695)	1695
Scan2Scan	MICCAI: GE → CAIN: GE (538) + MICCAI: Siemens → CAIN: GE (554) + MICCAI: Philips → CAIN: GE (603)	1695
Scan2Scan	MICCAI: GE → CAIN: Siemens (538) + MICCAI: Siemens → CAIN: Siemens (554) + MICCAI: Philips → CAIN: Siemens (603)	1695
Scan2Scan	MICCAI: GE → CAIN: Philips (538) + MICCAI: Siemens → CAIN: Philips (554) + MICCAI: Philips → CAIN: Philips (603)	1695
Label2Image	MICCAI: Labels → CAIN: GE (1695)	1695
Label2Image	MICCAI: Labels → CAIN: Siemens (1695)	1695
Label2Image	MICCAI: Labels → CAIN: Philips (1695)	1695
Syn2Image	Syn Labels → CAIN: GE (5000)	5000
Syn2Image	Syn Labels → CAIN: Siemens (5000)	5000
Syn2Image	Syn Labels → CAIN: Philips (5000)	5000
Mixed Target Distribution		
Image2Image	MICCAI → CAIN: GE (1695) + MICCAI → CAIN: Siemens (1695) + MICCAI → CAIN: Philips (1695)	5085
Scan2Scan	MICCAI: GE → CAIN: GE (538) + MICCAI: Siemens → CAIN: GE (554) + MICCAI: Philips → CAIN: GE (603) + MICCAI: GE → CAIN: Siemens (538) + MICCAI: Siemens → CAIN: Siemens (554) + MICCAI: Philips → CAIN: Siemens (603) + MICCAI: GE → CAIN: Philips (538) + MICCAI: Siemens → CAIN: Philips (554) + MICCAI: Philips → CAIN: Philips (603)	5085
Label2Image	MICCAI: Labels → CAIN: GE (1695) + MICCAI: Labels → CAIN: Siemens (1695) + MICCAI: Labels → CAIN: Philips (1695)	5085
Syn2Image	Syn Labels → CAIN: GE (5000) + Syn Labels → CAIN: Siemens (5000) + Syn Labels → CAIN: Philips (5000)	15000

Table 4: Summary of Synthetic Datasets for Segmentation Training

.3 Segmentation Performance

.3.1 TRAINING ON SINGLE DISTRIBUTION

Method	Dice	HD	AVD	L-Recall	L-F1	FPR (%)
Target: GE						
Lower	0.53±0.18	11.02±5.46	156.57±187.69	0.80±0.14	0.46±0.18	0.29±0.15
Upper	0.65±0.10	7.40±35.04	22.09±18.44	0.61±0.18	0.67±0.12	0.10±0.05
Image2Image	0.58±0.13	8.48±66.04	65.07±72.30	0.73±0.16	0.54±0.11	0.18±0.10
Scan2scan	0.58±0.12	9.14±72.25	73.72±56.91	0.78±0.13	0.51±0.10	0.22±0.11
Label2Image	0.59±0.09	9.99±72.13	41.16±31.69	0.75±0.13	0.56±0.12	0.17±0.07
Unsupervised	0.44±0.12	13.40±4.60	44.93±25.82	0.51±0.14	0.24±0.13	0.21±0.08
Target: Siemens						
Lower	0.59±0.06	19.50±5.49	35.50±24.62	0.66±0.15	0.47±0.09	0.07±0.03
Upper	0.69±0.07	11.93±9.75	32.90±28.80	0.61±0.15	0.56±0.14	0.13±0.09
Image2Image	0.59±0.07	17.07±7.21	31.82±15.62	0.58±0.19	0.51±0.12	0.05±0.02
Scan2scan	0.51±0.07	14.33±4.32	32.24±19.23	0.61±0.15	0.44±0.11	0.06±0.02
Label2Image	0.63±0.08	17.35±6.66	16.11±17.03	0.59±0.14	0.45±0.10	0.10±0.04
Unsupervised	0.37±0.14	24.21±4.30	37.54±17.59	0.29±0.12	0.19±0.05	0.08±0.04
Target: Philips						
Lower	0.57±0.13	23.94±9.25	83.75±131.35	0.73±0.18	0.60±0.12	0.10±0.10
Upper	0.60±0.09	14.44±6.30	62.79±42.44	0.75±0.18	0.69±0.07	0.08±0.07
Image2Image	0.52±0.14	28.46±14.09	85.85±149.31	0.49±0.18	0.50±0.10	0.09±0.10
Scan2scan	0.55±0.13	24.14±16.59	50.11±83.72	0.52±0.18	0.57±0.10	0.07±0.07
Label2Image	0.53±0.13	34.37±19.54	39.98±46.72	0.47±0.16	0.52±0.10	0.06±0.06
Unsupervised	0.32±0.13	37.37±12.24	40.24±30.56	0.31±0.17	0.25±0.04	0.06±0.08

Table 5: Training on Target Distribution

.3.2 TRAINING ON MIXED DISTRIBUTION

Method	Dice	HD	AVD	L-Recall	L-F1	FPR (%)
Target: GE						
Lower	0.53±0.18	11.01±5.46	156.57±187.69	0.80±0.14	0.46±0.18	0.29±0.15
Upper	0.65±0.10	7.65±4.17	31.94±27.51	0.67±0.21	0.69±0.10	0.11±0.04
Image2Image	0.58±0.13	9.02±4.71	73.91±73.19	0.74±0.17	0.53±0.10	0.19±0.11
Scan2scan	0.56±0.13	7.80±3.72	93.37±82.55	0.76±0.16	0.58±0.09	0.26±0.15
Label2Image	0.63±0.10	8.07±3.37	33.05±34.69	0.72±0.17	0.63±0.07	0.14±0.07
Syn2Im	0.40±0.14	16.44±6.77	34.20±28.59	0.23±0.10	0.33±0.11	0.13±0.07
Target: Siemens						
Lower	0.59±0.06	19.50±5.49	35.50±24.62	0.66±0.15	0.47±0.09	0.07±0.03
Upper	0.72±0.06	5.66±3.70	19.72±13.79	0.61±0.12	0.69±0.09	0.10±0.08
Image2Image	0.58±0.10	9.63±2.02	35.06±20.35	0.61±0.14	0.55±0.08	0.05±0.02
Scan2scan	0.59±0.08	8.64±5.14	32.53±18.14	0.65±0.15	0.59±0.09	0.07±0.03
Label2Image	0.64±0.08	15.70±7.74	22.17±16.13	0.62±0.11	0.48±0.10	0.07±0.03
Syn2Im	0.40±0.17	27.13±18.74	23.68±26.06	0.18±0.07	0.26±0.08	0.12±0.06
Target: Philips						
Lower	0.57±0.13	23.94±9.25	83.75±131.35	0.73±0.18	0.60±0.12	0.10±0.10
Upper	0.61±0.11	20.15±9.28	29.31±25.08	0.49±0.16	0.62±0.12	0.05±0.05
Image2Image	0.58±0.13	25.13±16.43	57.16±94.40	0.56±0.20	0.57±0.11	0.07±0.07
Scan2scan	0.54±0.10	18.89±9.90	54.48±89.86	0.65±0.18	0.62±0.11	0.08±0.09
Label2Image	0.58±0.12	25.34±20.01	42.72±51.90	0.60±0.20	0.61±0.10	0.06±0.06
Syn2Im	0.32±0.12	52.52±33.10	69.49±111.64	0.17±0.12	0.26±0.14	0.08±0.06

Table 6: Training on Mixed Distribution

References

- Amy Bearman, Olga Russakovsky, Vittorio Ferrari, and Li Fei-Fei. What’s the Point: Semantic Segmentation with Point Supervision. *arXiv:1506.02106 [cs]*, July 2016. URL <http://arxiv.org/abs/1506.02106>. arXiv: 1506.02106.
- Justin DiGregorio, Giordano Arezza, Adam Gibicar, Alan R. Moody, Pascal N. Tyrrell, and April Khademi. Intracranial volume segmentation for neurodegenerative populations using multicentre FLAIR MRI. *Neuroimage: Reports*, 1(1):100006, March 2021. ISSN 26669560. doi: 10.1016/j.ynirp.2021.100006. URL <https://linkinghub.elsevier.com/retrieve/pii/S2666956021000040>.
- Nicola K. Dinsdale, Mark Jenkinson, and Ana I.L. Namburete. Deep learning-based unlearning of dataset bias for MRI harmonisation and confound removal. *NeuroImage*, 228:117689, March 2021. ISSN 10538119. doi: 10.1016/j.neuroimage.2020.117689. URL <https://linkinghub.elsevier.com/retrieve/pii/S1053811920311745>.
- Christine Egger, Roland Opfer, Chenyu Wang, Timo Kepp, Maria Pia Sormani, Lothar Spies, Michael Barnett, and Sven Schippling. MRI FLAIR lesion segmentation in multiple sclerosis: Does automated segmentation hold up with manual annotation? *NeuroImage: Clinical*, 13:264–270, 2017.
- Brian Everitt and Anders Skrondal. *The Cambridge dictionary of statistics*, volume 106. Cambridge university press Cambridge, 2002.
- Maayan Frid-Adar, Eyal Klang, Michal Amitai, Jacob Goldberger, and Hayit Greenspan. Synthetic Data Augmentation using GAN for Improved Liver Lesion Classification. *arXiv:1801.02385 [cs]*, January 2018. URL <http://arxiv.org/abs/1801.02385>. arXiv: 1801.02385.
- Yaroslav Ganin, Evgeniya Ustinova, Hana Ajakan, Pascal Germain, Hugo Larochelle, François Laviolette, Mario Marchand, and Victor Lempitsky. Domain-Adversarial Training of Neural Networks. *arXiv:1505.07818 [cs, stat]*, May 2016. URL <http://arxiv.org/abs/1505.07818>. arXiv: 1505.07818.
- Mohsen Ghafoorian, Alireza Mehrtash, Tina Kapur, Nico Karssemeijer, Elena Marchiori, Mehran Pesteie, Charles R. G. Guttmann, Frank-Erik de Leeuw, Clare M. Tempny, Bram van Ginneken, Andriy Fedorov, Purang Abolmaesumi, Bram Platel, and William M. Wells III. Transfer Learning for Domain Adaptation in MRI: Application in Brain Lesion Segmentation. *arXiv:1702.07841 [cs]*, 10435:516–524, 2017. doi: 10.1007/978-3-319-66179-7_59. URL <http://arxiv.org/abs/1702.07841>. arXiv: 1702.07841.
- Ian Goodfellow, Jean Pouget-Abadie, Mehdi Mirza, Bing Xu, David Warde-Farley, Sherjil Ozair, Aaron Courville, and Yoshua Bengio. Generative adversarial nets. In *Advances in neural information processing systems*, pages 2672–2680, 2014.
- Arthur Gretton, Alex Smola, Jiayuan Huang, Marcel Schmittfull, Karsten Borgwardt, and Bernhard Schölkopf. Covariate Shift by Kernel Mean Matching. In Joaquin

- Quiñonero-Candela, Masashi Sugiyama, Anton Schwaighofer, and Neil D. Lawrence, editors, *Dataset Shift in Machine Learning*, pages 131–160. The MIT Press, December 2008. ISBN 978-0-262-17005-5. doi: 10.7551/mitpress/9780262170055.003.0008. URL <http://mitpress.universitypressscholarship.com/view/10.7551/mitpress/9780262170055.001.0001/upso-9780262170055-chapter-8>.
- Kaiming He, Xiangyu Zhang, Shaoqing Ren, and Jian Sun. Deep Residual Learning for Image Recognition. *arXiv:1512.03385 [cs]*, December 2015. URL <http://arxiv.org/abs/1512.03385>. arXiv: 1512.03385.
- Martin Heusel, Hubert Ramsauer, Thomas Unterthiner, Bernhard Nessler, and Sepp Hochreiter. GANs Trained by a Two Time-Scale Update Rule Converge to a Local Nash Equilibrium. *arXiv:1706.08500 [cs, stat]*, January 2018. URL <http://arxiv.org/abs/1706.08500>. arXiv: 1706.08500.
- Wei-Chih Hung, Yi-Hsuan Tsai, Yan-Ting Liou, Yen-Yu Lin, and Ming-Hsuan Yang. Adversarial Learning for Semi-Supervised Semantic Segmentation. *arXiv:1802.07934 [cs]*, July 2018. URL <http://arxiv.org/abs/1802.07934>. arXiv: 1802.07934.
- Yuankai Huo, Zhoubing Xu, Hyeonsoo Moon, Shunxing Bao, Albert Assad, Tamara K. Moyo, Michael R. Savona, Richard G. Abramson, and Bennett A. Landman. SynSeg-Net: Synthetic Segmentation Without Target Modality Ground Truth. *IEEE Transactions on Medical Imaging*, 38(4):1016–1025, April 2019. ISSN 1558-254X. doi: 10.1109/TMI.2018.2876633. Conference Name: IEEE Transactions on Medical Imaging.
- Phillip Isola, Jun-Yan Zhu, Tinghui Zhou, and Alexei A. Efros. Image-to-Image Translation with Conditional Adversarial Networks. *arXiv:1611.07004 [cs]*, November 2018. URL <http://arxiv.org/abs/1611.07004>. arXiv: 1611.07004.
- Jue Jiang, Yu-Chi Hu, Neelam Tyagi, Pengpeng Zhang, Andreas Rimner, Gig S. Mageras, Joseph O. Deasy, and Harini Veeraraghavan. Tumor-aware, Adversarial Domain Adaptation from CT to MRI for Lung Cancer Segmentation. *Medical image computing and computer-assisted intervention : MICCAI ... International Conference on Medical Image Computing and Computer-Assisted Intervention*, 11071:777–785, September 2018. doi: 10.1007/978-3-030-00934-2_86. URL <https://www.ncbi.nlm.nih.gov/pmc/articles/PMC6169798/>.
- Ian T. Jolliffe and Jorge Cadima. Principal component analysis: a review and recent developments. *Philosophical Transactions of the Royal Society A: Mathematical, Physical and Engineering Sciences*, 374(2065):20150202, April 2016. ISSN 1364-503X, 1471-2962. doi: 10.1098/rsta.2015.0202. URL <https://royalsocietypublishing.org/doi/10.1098/rsta.2015.0202>.
- Tero Karras, Samuli Laine, and Timo Aila. A Style-Based Generator Architecture for Generative Adversarial Networks. *arXiv:1812.04948 [cs, stat]*, March 2019. URL <http://arxiv.org/abs/1812.04948>. arXiv: 1812.04948.

- Tero Karras, Miika Aittala, Janne Hellsten, Samuli Laine, Jaakko Lehtinen, and Timo Aila. Training Generative Adversarial Networks with Limited Data. *arXiv:2006.06676 [cs, stat]*, October 2020. URL <http://arxiv.org/abs/2006.06676>. arXiv: 2006.06676.
- April Khademi, Adam Gibicar, Giordano Arezza, Justin DiGregorio, Pascal N. Tyrrell, and Alan R. Moody. Segmentation of white matter lesions in multicentre FLAIR MRI. *Neuroimage: Reports*, 1(4):100044, December 2021. ISSN 26669560. doi: 10.1016/j.ynirp.2021.100044. URL <https://linkinghub.elsevier.com/retrieve/pii/S2666956021000428>.
- Anna Khoreva, Rodrigo Benenson, Jan Hosang, Matthias Hein, and Bernt Schiele. Simple Does It: Weakly Supervised Instance and Semantic Segmentation. *arXiv:1603.07485 [cs]*, November 2016. URL <http://arxiv.org/abs/1603.07485>. arXiv: 1603.07485.
- Diederik P. Kingma and Jimmy Ba. Adam: A Method for Stochastic Optimization. *arXiv:1412.6980 [cs]*, January 2017. URL <http://arxiv.org/abs/1412.6980>. arXiv: 1412.6980.
- Hugo J. Kuijff, J. Matthijs Biesbroek, Jeroen de Bresser, Rutger Heinen, Simon Andermatt, Mariana Bento, Matt Berseth, Mikhail Belyaev, M. Jorge Cardoso, Adrià Casamitjana, D. Louis Collins, Mahsa Dadar, Achilleas Georgiou, Mohsen Ghafoorian, Dakai Jin, April Khademi, Jesse Knight, Hongwei Li, Xavier Lladó, Miguel Luna, Qaiser Mahmood, Richard McKinley, Alireza Mehrtash, Sébastien Ourselin, Bo-yong Park, Hyunjin Park, Sang Hyun Park, Simon Pezold, Elodie Puybareau, Leticia Rittner, Carole H. Sudre, Sergi Valverde, Verónica Vilaplana, Roland Wiest, Yongchao Xu, Ziyue Xu, Guodong Zeng, Jianguo Zhang, Guoyan Zheng, Christopher Chen, Wiesje van der Flier, Frederik Barkhof, Max A. Viergever, and Geert Jan Biessels. Standardized Assessment of Automatic Segmentation of White Matter Hyperintensities and Results of the WMH Segmentation Challenge. *IEEE Transactions on Medical Imaging*, 38(11):2556–2568, November 2019. ISSN 0278-0062, 1558-254X. doi: 10.1109/TMI.2019.2905770. URL <http://arxiv.org/abs/1904.00682>. arXiv: 1904.00682.
- Daiqing Li, Junlin Yang, Karsten Kreis, Antonio Torralba, and Sanja Fidler. Semantic Segmentation with Generative Models: Semi-Supervised Learning and Strong Out-of-Domain Generalization. *arXiv:2104.05833 [cs]*, April 2021. URL <http://arxiv.org/abs/2104.05833>. arXiv: 2104.05833.
- Jonathan Long, Evan Shelhamer, and Trevor Darrell. Fully Convolutional Networks for Semantic Segmentation. *arXiv:1411.4038 [cs]*, March 2015. URL <http://arxiv.org/abs/1411.4038>. arXiv: 1411.4038.
- Mario Lucic, Karol Kurach, Marcin Michalski, Sylvain Gelly, and Olivier Bousquet. Are GANs Created Equal? A Large-Scale Study. *arXiv:1711.10337 [cs, stat]*, October 2018. URL <http://arxiv.org/abs/1711.10337>. arXiv: 1711.10337.
- Julian Alberto Palladino, Diego Fernandez Slezak, and Enzo Ferrante. Unsupervised Domain Adaptation via CycleGAN for White Matter Hyperintensity Segmentation in Multicenter MR Images. *arXiv:2009.04985 [cs, eess]*, September 2020. URL <http://arxiv.org/abs/2009.04985>. arXiv: 2009.04985.

- Chris H Polman, Stephen C Reingold, Brenda Banwell, Michel Clanet, Jeffrey A Cohen, Massimo Filippi, Kazuo Fujihara, Eva Havrdova, Michael Hutchinson, Ludwig Kappos, and others. Diagnostic criteria for multiple sclerosis: 2010 revisions to the McDonald criteria. *Annals of neurology*, 69(2):292–302, 2011.
- Xiaojuan Qi, Zhengzhe Liu, Jianping Shi, Hengshuang Zhao, and Jiaya Jia. Augmented Feedback in Semantic Segmentation Under Image Level Supervision. In Bastian Leibe, Jiri Matas, Nicu Sebe, and Max Welling, editors, *Computer Vision – ECCV 2016*, volume 9912, pages 90–105. Springer International Publishing, Cham, 2016. ISBN 978-3-319-46483-1 978-3-319-46484-8. doi: 10.1007/978-3-319-46484-8_6. URL http://link.springer.com/10.1007/978-3-319-46484-8_6. Series Title: Lecture Notes in Computer Science.
- Alec Radford, Luke Metz, and Soumith Chintala. Unsupervised Representation Learning with Deep Convolutional Generative Adversarial Networks. *arXiv:1511.06434 [cs]*, January 2016. URL <http://arxiv.org/abs/1511.06434>. arXiv: 1511.06434.
- Brittany Reiche, A.R. Moody, and April Khademi. Pathology-preserving intensity standardization framework for multi-institutional FLAIR MRI datasets. *Magnetic Resonance Imaging*, 62:59–69, October 2019. ISSN 0730725X. doi: 10.1016/j.mri.2019.05.001. URL <https://linkinghub.elsevier.com/retrieve/pii/S0730725X18304120>.
- Olaf Ronneberger, Philipp Fischer, and Thomas Brox. U-Net: Convolutional Networks for Biomedical Image Segmentation. *arXiv:1505.04597 [cs]*, May 2015. URL <http://arxiv.org/abs/1505.04597>. arXiv: 1505.04597.
- Veit Sandfort, Ke Yan, Perry J. Pickhardt, and Ronald M. Summers. Data augmentation using generative adversarial networks (CycleGAN) to improve generalizability in CT segmentation tasks. *Scientific Reports*, 9(1):16884, December 2019. ISSN 2045-2322. doi: 10.1038/s41598-019-52737-x. URL <http://www.nature.com/articles/s41598-019-52737-x>.
- Maximilian Seitzer. pytorch-fid: FID Score for PyTorch, August 2020. URL <https://github.com/mseitzer/pytorch-fid>.
- Ashish Shrivastava, Tomas Pfister, Oncel Tuzel, Josh Susskind, Wenda Wang, and Russ Webb. Learning from Simulated and Unsupervised Images through Adversarial Training. *arXiv:1612.07828 [cs]*, July 2017. URL <http://arxiv.org/abs/1612.07828>. arXiv: 1612.07828.
- Martijn D. Steenwijk, Petra J.W. Pouwels, Marita Daams, Jan Willem van Dalen, Matthan W.A. Caan, Edo Richard, Frederik Barkhof, and Hugo Vrenken. Accurate white matter lesion segmentation by k nearest neighbor classification with tissue type priors (kNN-TTPs). *NeuroImage: Clinical*, 3:462–469, 2013. ISSN 22131582. doi: 10.1016/j.nicl.2013.10.003. URL <https://linkinghub.elsevier.com/retrieve/pii/S2213158213001332>.

- Carole H. Sudre, Wenqi Li, Tom Vercauteren, Sébastien Ourselin, and M. Jorge Cardoso. Generalised Dice overlap as a deep learning loss function for highly unbalanced segmentations. *arXiv:1707.03237 [cs]*, 10553:240–248, 2017. doi: 10.1007/978-3-319-67558-9_28. URL <http://arxiv.org/abs/1707.03237>. arXiv: 1707.03237.
- Vaanathi Sundaresan, Giovanna Zamboni, Nicola K. Dinsdale, Peter M. Rothwell, Ludovica Griffanti, and Mark Jenkinson. Comparison of domain adaptation techniques for white matter hyperintensity segmentation in brain MR images. preprint, Neuroscience, March 2021. URL <http://biorxiv.org/lookup/doi/10.1101/2021.03.12.435171>.
- Jean-Claude Tardif, J. David Spence, Therese M. Heinonen, Alan Moody, Josephine Presacco, Richard Frayne, Philippe L’Allier, Benjamin J.W. Chow, Matthias Friedrich, Sandra E. Black, Aaron Fenster, Brian Rutt, and Rob Beanlands. Atherosclerosis Imaging and the Canadian Atherosclerosis Imaging Network. *Canadian Journal of Cardiology*, 29(3):297–303, March 2013. ISSN 0828282X. doi: 10.1016/j.cjca.2012.09.017. URL <https://linkinghub.elsevier.com/retrieve/pii/S0828282X12013694>.
- Laurens Van der Maaten and Geoffrey Hinton. Visualizing data using t-SNE. *Journal of machine learning research*, 9(11), 2008.
- Stefan Van der Walt, Johannes L Schönberger, Juan Nunez-Iglesias, François Boulogne, Joshua D Warner, Neil Yager, Emmanuelle Gouillart, and Tony Yu. scikit-image: image processing in Python. *PeerJ*, 2:e453, 2014.
- Riccardo Volpi, Hongseok Namkoong, Ozan Sener, John Duchi, Vittorio Murino, and Silvio Savarese. Generalizing to unseen domains via adversarial data augmentation. *arXiv preprint arXiv:1805.12018*, 2018.
- Joanna M Wardlaw, Maria C Valdés Hernández, and Susana Muñoz-Maniega. What are White Matter Hyperintensities Made of? *Journal of the American Heart Association: Cardiovascular and Cerebrovascular Disease*, 4(6):e001140, June 2015. ISSN 2047-9980. doi: 10.1161/JAHA.114.001140. URL <https://www.ncbi.nlm.nih.gov/pmc/articles/PMC4599520/>.
- Garrett Wilson and Diane J. Cook. A Survey of Unsupervised Deep Domain Adaptation. *arXiv:1812.02849 [cs, stat]*, February 2020. URL <http://arxiv.org/abs/1812.02849>. arXiv: 1812.02849.
- Jelmer M. Wolterink, Anna M. Dinkla, Mark H. F. Savenije, Peter R. Seevinck, Cornelis A. T. van den Berg, and Ivana Isgum. Deep MR to CT Synthesis using Unpaired Data. *arXiv:1708.01155 [cs]*, August 2017. URL <http://arxiv.org/abs/1708.01155>. arXiv: 1708.01155.
- Kaichao You, Mingsheng Long, Jianmin Wang, and Michael I. Jordan. How Does Learning Rate Decay Help Modern Neural Networks? *arXiv:1908.01878 [cs, stat]*, September 2019. URL <http://arxiv.org/abs/1908.01878>. arXiv: 1908.01878.
- Jan Zenisek, Florian Holzinger, and Michael Affenzeller. Machine learning based concept drift detection for predictive maintenance. *Computers & Industrial Engineering*, 137:

106031, November 2019. ISSN 03608352. doi: 10.1016/j.cie.2019.106031. URL <https://linkinghub.elsevier.com/retrieve/pii/S0360835219304905>.

Yuxuan Zhang, Huan Ling, Jun Gao, Kangxue Yin, Jean-Francois Lafleche, Adela Barriuso, Antonio Torralba, and Sanja Fidler. DatasetGAN: Efficient Labeled Data Factory with Minimal Human Effort. *arXiv:2104.06490 [cs]*, April 2021. URL <http://arxiv.org/abs/2104.06490>. arXiv: 2104.06490.

Zizhao Zhang, Lin Yang, and Yefeng Zheng. Translating and Segmenting Multimodal Medical Volumes with Cycle- and Shape-Consistency Generative Adversarial Network. *arXiv:1802.09655 [cs]*, March 2019. URL <http://arxiv.org/abs/1802.09655>. arXiv: 1802.09655.

Yi Zhong, Shouliang Qi, Yan Kang, Wei Feng, and E. Mark Haacke. Automatic skull stripping in brain MRI based on local moment of inertia structure tensor. In *2012 IEEE International Conference on Information and Automation*, pages 437–440, Shenyang, China, June 2012. IEEE. ISBN 978-1-4673-2237-9 978-1-4673-2238-6 978-1-4673-2236-2. doi: 10.1109/ICInfA.2012.6246845. URL <http://ieeexplore.ieee.org/document/6246845/>.

Jun-Yan Zhu, Taesung Park, Phillip Isola, and Alexei A. Efros. Unpaired Image-to-Image Translation using Cycle-Consistent Adversarial Networks. *arXiv:1703.10593 [cs]*, August 2020. URL <http://arxiv.org/abs/1703.10593>. arXiv: 1703.10593.